J|A|C|S
ARTICLES
Published on Web 05/03/2002

Thin-Film Solid-State Electroluminescent Devices Based On Tris(2,2′-bipyridine)ruthenium(II) Complexes

Mihai Buda, Gregory Kalyuzhny, and Allen J. Bard*

Contribution from the Department of Chemistry and Biochemistry and Center for Nano- and Molecular Science and Technology, The University of Texas at Austin, Austin, Texas 78712

Received December 20, 2001

Abstract: The behavior of light-emitting electrochemical cells (LEC) based on solid films (~100 nm) of tris(2,2′-bipyridine)ruthenium(II) between an ITO anode and a Ga−In cathode was investigated. The response times were strongly influenced by the nature of the counterion: small anions (BF_4^- and ClO_4^-) led to relatively fast transients, while large anions (PF_6^-, AsF_6^-) produced a slow time-response. From comparative experiments of cells prepared and tested in a glovebox to those in ambient, mobility of the anions in these films appears to be related to the presence of traces of water from atmospheric moisture. An electrochemical model is proposed to describe the behavior of these LECs. The simulation results agreed well with experimental transients of current and light emission as a function of time and show that the charge injection is asymmetric at the two electrodes. At a small bias, electrons are the major carriers, while for a larger bias the conduction becomes bipolar.

Introduction

Organic light-emitting devices based on tris(2,2′-bipyridine)-ruthenium(II) complexes are promising candidates for high-efficiency, low-voltage devices. Although there is vast literature dealing with organic light-emitting diodes based on polymers and Alq_3, solid-state electroluminescent devices based on inorganic salts such as $Ru(bpy)_3^{2+}$ as the active substrate have only recently been investigated in detail[1,2] (although the first paper describing a light-emitting device based on a ruthenium phenanthroline complex was published in 1996[3]). Basically, a thin film (~100 nm) of $Ru(bpy)_3X_2$ (where X is an anion like ClO_4^- or BF_4^-) is deposited by spin coating on an indium tin oxide (ITO) substrate, and a metal contact is formed on the top. Over the past years, organic light-emitting devices that incorporate mobile ions have been referred to as organic light-emitting electrochemical cells (LECs), in contrast to OLEDs that behave more as solid-state semiconductor devices.[4,5] OLEDs behave analogously to solid-state semiconductor devices. There are a negligible number of mobile ions in the film, and charge injection requires ohmic contacts at the electrodes. LECs involve films in which there are mobile ions, and charge injection is relatively independent of the nature of the contacts. In both cases, however, chemical reactions at the contacts can occur, and these can produce deleterious effects on the cell operation. There are several important features that distinguish LECs from conventional OLEDs: (1) The "turn-on" voltage of LECs is close to the optical gap and is only very weakly dependent on the film thickness. (2) The quantum efficiencies of LECs do not depend on the electrode work-function. (3) LECs exhibit symmetrical current−voltage and light−voltage characteristics.

All of the above characteristics are observed for tris(2,2′-bipyridine)ruthenium salt light-emitting devices, suggesting that these devices are, in fact, LECs.

In the present paper, we report the general behavior of these light-emitting devices and demonstrate that the response depends critically on the nature of the anion and whether the cell is prepared and tested in the ambient or in an inert atmosphere box. We propose an electrochemical model and show simulation results that correlate well with the observed behavior of these cells.

Experimental Section

$Ru(bpy)_3(ClO_4)_2$ was prepared by a metathesis reaction between commercial $Ru(bpy)_3Cl_2$ (Aldrich) and excess sodium perchlorate.[6] The resulting crystals were recrystallized from acetonitrile/benzene and dried under vacuum at ~100 °C for several hours. $Ru(bpy)_3(BF_4)_2$, $Ru(bpy)_3(PF_6)_2$, and $Ru(bpy)_3(AsF_6)_2$ were prepared using similar procedures with the appropriate sodium or ammonium salts.

ITO covered glass (~20 Ω/□, Delta Technologies) was thoroughly cleaned before device preparation by sonication for 20 min in a 20% (vol) solution of ethanolamine in highly pure Millipore water at ~60 °C, followed by three rinsing/sonication steps with pure water at room temperature to remove traces of ethanolamine, and drying under vacuum for several hours at ~80 °C.

$Ru(bpy)_3(X)_2$ solutions in acetonitrile were always filtered through 0.2 μm syringe filters before use. Typically, the $Ru(bpy)_3(X)_2$ films (~100 nm) were spin-coated (Headway Research) from a 4% (w/v) acetonitrile solution at 2000 rpm, onto clean ITO covered glass. After spin coating, the device was dried under vacuum for at least 8 h at

* To whom correspondence should be addressed. E-mail: ajbard@mail.utexas.edu.

(1) Handy, E. S.; Pal, A. J.; Rubner, M. F. *J. Am. Chem. Soc.* **1999**, *121*, 3525.
(2) Gao, F. G.; Bard, A. J. *J. Am. Chem. Soc.* **2000**, *122*, 7426.
(3) Lee, J.-K.; Yoo, D. S.; Handy, E. S.; Rubner, M. F. *Appl. Phys. Lett.* **1996**, *69*, 1686.
(4) Mitschke, U.; Bäuerle, P. *J. Mater. Chem.* **2000**, *10*, 1471.
(5) Pei, Q.; Yang, Y. *Synth. Met.* **1996**, *80*, 131.
(6) McCord, P.; Bard, A. J. *J. Electroanal. Chem.* **1991**, *318*, 91.

10.1021/ja017834h CCC: $22.00

~120 °C. Ga−Sn or Ga−In (Alfa-Aesar) liquid contacts were printed using a syringe, while Au contacts were evaporated on top of the film. The current−light emission−voltage curves were taken using an AUTOLAB electrochemical station coupled with a Newport optical power-meter. Measurements were performed under ambient conditions at room temperature (25 °C), or in a drybox under a nitrogen atmosphere. For the measurements performed in the drybox, the films were spin-coated, dried, and tested under nitrogen in the same drybox, without being exposed to air.

All experimental data were taken under ambient conditions, unless otherwise specified. A typical cell structure can be found in ref 2; all measurements were performed using a similar cell, without the epoxy coating.

All simulations were run on a 650 MHz PC under MS Windows Millenium. The Fortran sources were compiled using the GNU g77 (Windows 32 version) compiler.

Results and Discussion

As already shown,[2] the emission spectrum of these electroluminescent devices is rather broad and centered at about 660 nm (red-orange light); the external quantum efficiency of these devices can reach 2.5%, while the maximum luminance can be as high as 2000 cd/m^2. The emission mechanism is probably similar to that for electrogenerated chemiluminescence of Ru(bpy)$_3^{2+}$ in solution (see, e.g., ref 6):

$$\mathrm{Ru(bpy)_3^{2+} + e^- \rightarrow Ru(bpy)_3^{+}}$$

$$\mathrm{Ru(bpy)_3^{2+} \rightarrow Ru(bpy)_3^{3+} + e^-}$$

$$\mathrm{Ru(bpy)_3^{+} + Ru(bpy)_3^{3+} \rightarrow Ru(bpy)_3^{2+} + Ru(bpy)_3^{2+}*}$$

$$\mathrm{Ru(bpy)_3^{2+}* \rightarrow Ru(bpy)_3^{2+} + h\nu}$$

where Ru(bpy)$_3^+$ can best be described as an electron localized on the bpy ligands, and Ru(bpy)$_3^{3+}$ represents an oxidized Ru center (throughout the paper in our discussion of processes in the solid, Ru(bpy)$_3^+$ species will be referred as "electrons" and Ru(bpy)$_3^{3+}$ species as "holes").

Typical response curves (current and light emission vs potential) of an (+)ITO/Ru(bpy)$_3$(ClO$_4$)$_2$/GaSn(−) device are shown in Figure 1a. On reversing the bias (− on ITO), no light was seen, but a relatively large current flowed because of the oxidation of the GaSn contact (not shown). If the GaSn liquid contact is replaced with a more inert contact, such as Au, essentially symmetrical characteristics are observed (Figure 1b). Similar symmetric characteristics were obtained using a carbon-paste contact instead of Au.

Transient Behavior. The transient behavior of these devices is strongly influenced by the mobility of the counterion (Figure 2). Small, mobile anions such as BF_4^- and ClO_4^- led to relatively fast transients (Figure 2a, b), while for large anions (PF_6^-, AsF_6^-), the time-response became very slow (Figure 2c, d). Thus, by changing the anion, response times were varied over several orders of magnitude. Similar slow responses have been observed for tris(bipyridyl)ruthenium light-emitting devices using PF_6^- as counterion.[1]

The influence of the anion mobility can also be clearly seen in the zero-bias impedance spectra (Figure 3). At zero bias, the film resistance is related to the mobility of the anions, since no other mobile species exist in the film (the Ru(bpy)$_3^{2+}$ sites are assumed to be fixed). For the Ru(bpy)$_3$(PF$_6$)$_2$ and Ru(bpy)$_3$(AsF$_6$)$_2$ films (the latter is not shown), which have low anion mobility and therefore show very large resistances, the impedance was an almost perfect vertical line, corresponding to the geometric capacitance of the film. For Ru(bpy)$_3$(BF$_4$)$_2$ films, which show high anion mobility and low resistances, the impedance consisted of a high-frequency circular arc and a low-frequency almost vertical line, characteristic of a thin film sandwiched between two blocking electrodes.[7] The case of Ru(bpy)$_3$(ClO$_4$)$_2$ films was intermediate, with only a circular arc observed. From the impedance data, one can estimate the resistivities of the films to be ~1.2 × 10^8 Ω cm for BF_4^- and ~1.6 × 10^9 Ω cm for ClO_4^-.

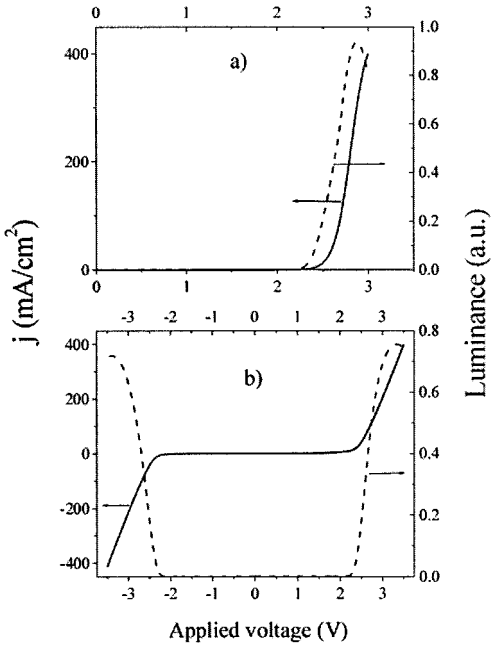

Figure 1. Current−voltage and light−voltage characteristics for (+)ITO/Ru(bpy)$_3$(ClO$_4$)$_2$/GaSn(−) (a) and ITO/Ru(bpy)$_3$(ClO$_4$)$_2$/Au (b) devices.

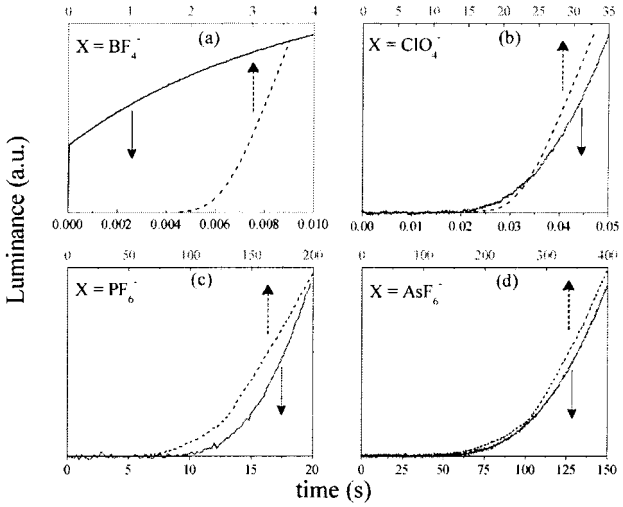

Figure 2. Luminance transients for a ITO/Ru(bpy)$_3$(X$^-$)$_2$/GaSn (100 nm, 2.5 V) device in air (−) and drybox (− − −). X$^-$ = (a) BF_4^-; (b) ClO_4^-; (c) PF_6^-; (d) AsF_6^-.

To obtain meaningful experimental data for both transient and impedance measurements, the devices must be free of shorts,

(7) Macdonald, J. R. *J. Chem. Phys.* **1974**, *61*, 3977.

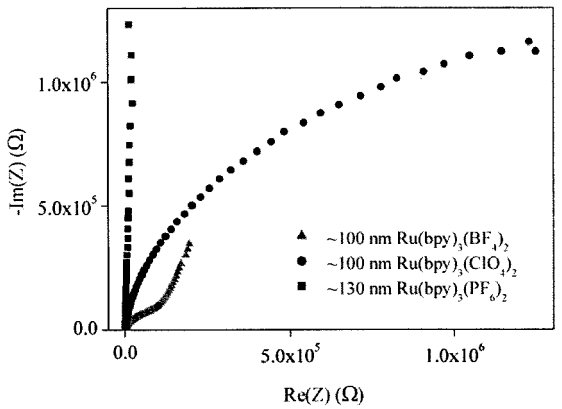

Figure 3. Typical zero-bias impedance spectra for $Ru(bpy)_3(X^-)_2$ ($A \approx 0.008$ cm^2, 1 MHz−100 Hz).

which give rise to leakage current. Leakage current associated with pinholes in the film yields nonreproducible results and questionable experimental data, especially when one needs to look at relatively small currents (i.e., at small applied bias). Devices made with evaporated contacts, such as Au and Al, are almost never free of shorts, particularly when using spin-coated films, and, therefore, are extremely difficult to analyze. On the other hand, liquid metal contacts readily produce short-free devices, since they do not easily penetrate the small pinholes that might be present in the film. By using such contacts one can obtain very reproducible results, despite some uncertainty in the active contact area. In a recent paper,[8] Rubner and Rudmann report a resistance as low as 1 kΩ for ITO/$Ru(bpy)_3(PF_6)_2$/Al devices at zero-bias, suggesting a small, but finite, number of shorts in such devices with evaporated Al contacts (although the same reference indicates that evaporated silver contacts lead to short-free devices as well). Note that for our devices (Figure 3), the zero-bias resistance of the ∼100 nm $Ru(bpy)_3(PF_6)_2$ film was actually too large to be measured accurately.

The existence of mobile ions in these films seems to be related, at least in part, to the presence of traces of either solvent or water from atmospheric moisture. Figure 2 also shows a comparison between devices prepared and tested both under ambient atmospheric conditions versus those made and tested in a nitrogen-filled drybox. While the general shape of the curves is the same, the devices prepared and tested in the drybox show a much longer response time. This behavior indicates that either the concentration of mobile ions or their mobility (or both) is smaller, and suggests that these films contain less residual solvent or water. Because the devices are prepared in the same way, except that they are not exposed to air, traces of water, rather than acetonitrile, are probably present in devices prepared under atmospheric conditions. Moreover, devices prepared in the drybox (spin coating and heating in a vacuum oven) and tested after being left in air for 2 days show the same behavior as the ones prepared in air, that is, shorter response times. Even devices prepared under an inert, dry atmosphere may still have some traces of water. Figure 2 also shows that the differences in response time between the two sets of data tend to become less important as the size of the counterion increases. The response times are several orders of magnitude larger for a "dry" device containing BF_4^-; the difference for a similar device containing AsF_6^- is only about 3−4 times, suggesting that traces of water are more likely to be found in films containing small, more hydrophilic counterions. For BF_4^- and ClO_4^- (for which the ion movement is fast enough to attain a steady state within a reasonable time), both the luminescence and the current density are about 5−10 times smaller than in air, while the quantum efficiency is about the same.

In an attempt to understand the transient behavior better, we have constructed and tested an electrochemical model of these devices, which despite its simplicity, can explain and predict experimental data. Several early attempts have been made to simulate the steady-state characteristics of LECs;[9−11] the transient behavior of these devices has received, however, less attention.[12] A somewhat less rigorous approach for characterizing transients of rubrene electroluminescence in thin-layer solution-phase electrolytic cells has been described.[13]

Model Description. The data presented above describing these cells show that the light-emitting devices based on $Ru(bpy)_3^{2+}$ salts as emitters behave like solid-state light-emitting electrochemical cells, in which charge injected by electrochemical reactions at the electrodes depends on the motion of counterions. Essentially, the main characteristic of LECs is the presence of mobile ions that allow the buildup of large electric fields near the electrodes and, consequently, the injection of charge at low applied voltages. In solution, numerous studies have shown that even very low ionic concentrations are still large enough to operate a light-emitting device.[14]

In the amorphous film of the solid-state device, the bulky $Ru(bpy)_3^{2+}$ sites are considered to be fixed, and only the counterions, X^-, are mobile. Moreover, we also assume that only a fraction of the anions are mobile; that is, the concentration of mobile anions is smaller than the total concentration of anions. This may be a function of the different solvation of the anions as suggested above or to different sites occupied by the anions (the film may be nanocrystalline, and only the regions near the boundaries between the small particles would provide mobile ions). We considered the device to be described by the Gouy−Chapman−Stern model;[15] the recombination term is taken as a second-order chemical reaction between electrons and holes. (A more detailed description of the model and the numerical method employed can be found in the Supporting Information.) A similar treatment for LECs has been proposed,[12] but in our approach, the interface at the two electrodes is treated within an electrochemical formalism rather than using the Fowler−Nordheim equation. Also, in our treatment the more general case of a slow electrode reaction can be readily accommodated.

Assumptions and Approximations. (1) The main assumption is the validity of the Gouy−Chapman−Stern model for describing the interfaces near each electrode, which has several limitations. (2) The carriers' flux equations are described by the Nernst−Planck equations (we assume that the carrier

(8) Rudmann, H.; Rubner, M. F. *J. Appl. Phys.* **2001**, *90*, 4338.
(9) Manzanares, M. F.; Reiss, H.; Heeger, A. J. *J. Phys. Chem.* **1998**, *102*, 4327.
(10) Smith, D. L. *J. Appl. Phys.* **1997**, *81*, 2869.
(11) Riess, I.; Cahen, D. *J. Appl. Phys.* **1997**, *82*, 3147.
(12) deMello, J. C.; Tessler, N.; Graham, S. C.; Friend, R. H. *Phys. Rev. B* **1998**, *57*, 12951.
(13) Orlik, M.; Doblhofer, K.; Ertl, G. *J. Phys. Chem.* **1998**, *102*, 6367.
(14) Schaper, H.; Köstlin, H.; Schnedler, E. *J. Electrochem. Soc.* **1982**, *129*, 1289.
(15) Bard, A. J.; Faulkner, L. R. *Electrochemical Methods*; Wiley: New York, 2001; p 546.

Table 1. Estimated Potential Barriers for Charge Injection in the $Ru(bpy)_3^{2+}$ Light-Emitting Devices

reduction potential (ACN vs Fc/Fc^+, V)	−1.698
oxidation potential (ACN vs Fc/Fc^+, V)	0.973
absolute reduction potential (V)	3.11
absolute oxidation potential (V)	5.78
estimated cathodic "potential barrier" in thin-film device (V)	−1.01
estimated anodic "potential barrier" in thin-film device (V)	1.38

concentrations are small compared to the total concentration of $Ru(bpy)_3^{2+}$ sites). (3) The film is treated as a continuous medium, without taking into account the size of the ions. (4) Mobilities and diffusion coefficients are related through the Einstein equation. (5) The total number of mobile ions is constant and does not depend on the field or the local concentrations of electrons and holes. (6) Mobilities of electrons and holes are field independent. (7) Activity coefficients are considered to be constant throughout the film at all times.

Interfaces and Charge Injection. In the Gouy−Chapman−Stern model of the electrode interface, a compact layer is considered to exist near the electrode. At the electrodes the following reactions take place:

$$A + e^- (M) \rightarrow R \text{ (cathode)}$$

$$A \rightarrow O + e^- (ITO) \text{ (anode)}$$

where R and O are the reduced (electrons or +1 Ru) and oxidized (holes of +3 Ru) species, respectively. By writing the electrochemical equilibrium condition for the two electrodes, one obtains the well-known Nernst equation (see the Supporting Information for more details):

$$\Phi_c - \Phi_c^0 = \Delta\Phi_c = \frac{1}{F}(\mu_A^0 + \mu_{e1}^0 - \mu_R^0) + \frac{RT}{F}\ln\frac{a_A}{a_R}$$

$$\Phi_a - \Phi_a^0 = \Delta\Phi_a = \frac{1}{F}(\mu_O^0 + \mu_{e2}^0 - \mu_A^0) + \frac{RT}{F}\ln\frac{a_O}{a_A} \quad (1)$$

where μ_i^0 are the chemical potentials of each species (A, R, O, and electrons). The differences $\mu_A^0 - \mu_R^0$ and $\mu_O^0 - \mu_A^0$ can be estimated from the reduction/oxidation potentials of $Ru(bpy)_3^{2+}$, while the chemical potential of electrons in the metal and ITO phases in the absence of any interactions between the contact and the film can be expressed as

$$\mu_e^0 = -\Psi_M \quad (2)$$

where Ψ_M is the work function of the metal electrode. Estimated results for the charge injection potential barriers at the electrodes, based on the absolute potential value for ferrocene, $\Phi_{Fc} = 4.81$,[16] work function of ITO, $\Psi_{ITO} = 4.4$,[17] and work function of GaIn liquid alloy, $\Psi_{GaIn} = 4.12$,[18] are shown in Table 1. The results in Table 1 show that the potential barrier for electron injection is slightly lower than that corresponding to hole injection for $Ru(bpy)_3^{2+}$ devices. However, the estimated potential barriers are only approximate; relating the work function of the metal to the chemical potential of electrons in the metal phase neglects the possible interactions between the metal contact and the film, while the work function of ITO depends on the precleaning procedure.[19] Moreover, gallium-based liquid alloys tend to form a thin layer of oxide in air, so the work function of this contact might be slightly larger. Therefore, for practical reasons, it is easier to describe the individual charge injection potential barriers $V_c^0 = (\mu_A^0 + \mu_{e1}^0 - \mu_R^0)/F$ and $V_a^0 = (\mu_O^0 + \mu_{e2}^0 - \mu_A^0)/F$ in terms of the total band gap. The band gap is equal to

$$V_b = V_a^0 - V_c^0 = \frac{1}{F}(\mu_O^0 + \mu_{e2}^0 - \mu_A^0 - \mu_A^0 - \mu_{e1}^0 + \mu_R^0) \approx \frac{1}{F}(\mu_O^0 - 2\mu_A^0 + \mu_R^0) \quad (3)$$

if one neglects the difference in electron chemical potentials between the two contacts (actually, Figure 1b shows that the nature of the contact at which the electrode reactions occur is not important). Now one can define the individual charge injection potential barriers by introducing a parameter, ν, $0 < \nu < 1$:

$$V_c^0 = -\nu V_b; \quad V_a^0 = (1 - \nu)V_b \quad (4)$$

to allow for asymmetrical barriers. A more detailed description of the metal/organic interface can be found in ref 20. The parameter ν basically describes how the total applied potential is distributed as a potential drop across the Helmholtz layers of the anode and cathode.

Model Equations. Once the model framework has been defined, one can write the Nernst−Planck flux equations and continuity equations for each mobile ionic species, coupled with Poisson's equation as follows.

(1) Flux equations for each mobile species (the diffusion coefficients and mobilities are assumed to obey Einstein's equation):

$$f_i(x,t) = -D_i\left(\frac{\partial c_i(x,t)}{\partial x} - z_i c_i(x,t)\frac{F}{RT}E(x,t)\right), \quad i = p, n, a \quad (5)$$

(2) Continuity equations:

$$\frac{\partial c_i(x,t)}{\partial t} = -\frac{\partial f_i(x,t)}{\partial x} - k \times c_p c_n, \begin{cases} k \neq 0, i = p, n \\ k = 0, i = a \end{cases} \quad (6)$$

(3) Poisson equation:

$$\frac{\partial E(x,t)}{\partial x} = \frac{1}{\epsilon\epsilon_0}\sum_i z_i c_i(x,t), \; i = n,p,a,r; \quad \frac{\partial \Phi(x,t)}{\partial x} = -E(x,t) \quad (7)$$

where the letters p, n, a, and r refer to holes (Ru^{III} sites), electrons (Ru^{I} sites), mobile anions, and fixed cations, respectively. $f_i(x,t)$, $c_i(x,t)$, and z_i are the fluxes, concentrations, and

(16) Richardson, D. E. *Inorg. Chem.* **1990**, *29*, 3213.
(17) Kugler, T.; Salaneck, W. R.; Rost, H.; Holmes, A. B. *Chem. Phys. Lett.* **1999**, *310*, 391.
(18) Emets, V. V.; Damaskin, B. B. *J. Electroanal. Chem.* **2000**, *491*, 30.
(19) Schlaf, R.; Murata, H.; Kafafi, Z. H. *J. Electron Spectrosc. Relat. Phenom.* **2001**, *120*, 149.
(20) Ishii, H.; Sugiyama, K.; Ito, E.; Seki, K. *Adv. Mater.* **1999**, *11*, 605.

charges of species i, k is the electron−hole recombination rate constant, $\Phi(x,t)$ is the electric potential, and $E(x,t)$ is the electric field.

The current flowing through the film is given by

$$I = F\sum_{i=p,n,a} z_i f_i(x,t) + \epsilon\epsilon_0 \frac{\partial E(x,t)}{\partial t} \quad (8)$$

where the second term represents the Maxwell displacement current and may be viewed as a capacitive current that vanishes at steady state.

Although the electrons and holes move throughout the film by electron-hopping between two adjacent sites and the system may be better described using the electron-hopping formalism developed by Savéant,[21] the numerical solution is more complicated in this case (see the Supporting Information).

Savéant showed that for electron-hopping between fixed sites, the migration term should contain a second-order term in concentration, $c(1 - c/c^0)$, where c^0 is the total concentration of electroactive centers. For low carrier concentration, $c \ll c^0$, the second-order term reduces to simply c, and hence the Savéant equation reduces to the Nernst−Planck equation. (Possibly due to a typographical error, the fluxes in the original paper (ref 21) are written without the $\partial\varphi/\partial$x term.) This can be more intuitively explained by the fact that any second-order process, such as the electron exchange between two sites, tends to become a pseudo-first-order process if the concentration of one "reactant" (site) is very large.

If one takes for the electron diffusion coefficient a value of about 10^{-7} cm^2/s[22] and assumes that the total current in our device is purely diffusional, from the steady-state current density due to both carriers, $i = 2(FDc^0/(L/2)$, one would obtain a value of about 6 A/cm^2 assuming $c^0 = 1.5$ M for a 100 nm film (actually, from Figure 2a one might estimate that the diffusion coefficient of electrons for films made in air is about an order of magnitude larger, so it is likely that the estimated current value may be even larger). The largest current density observed experimentally for films made in air does not exceed ∼400−450 mA/cm^2 (Figure 1), so the maximum carrier concentration should not exceed $\sim 0.07c^0$, indicating that the second-order correction is small. Moreover, even at 3.0 V the simulations never show a carrier concentration larger than about $\sim 0.06c^0$, proving that the approximation holds well. We, therefore, consider that for the voltage range of practical interest for these devices, the Nernst−Planck equation is a reasonable approximation.

Initial and Boundary Conditions. Three sets of boundary conditions can be written for each electrode: two conditions for the concentration of electrons and holes at the electrode, one condition for the anionic flux, and one condition for electric-field continuity at the compact layer/active film boundary as follows:

(1) The Nernst equation for the concentrations of species at the electrode (a fast electrode heterogeneous electron-transfer reaction is assumed):

$$\Delta\Phi_c = \Phi_c - \Phi_c^0 = V_c^0 + \frac{RT}{F}\ln\left(\frac{c^* - c_n(0,t) - c_p(0,t)}{c_n(0,t)}\right) = V_a^0 + \frac{RT}{F}\ln\left(\frac{c_p(0,t)}{c^* - c_n(0,t) - c_p(0,t)}\right) \quad (9)$$

(2) Blocking-electrode conditions for the counterions at both electrodes (i.e., zero-flux condition, since the anions are considered to be inert and are not involved in any electrode reaction):

$$\left(\frac{\partial c_a(x,t)}{\partial x}\right)_{x=0} - c_a(0,t)\frac{F}{RT}\left(\frac{\partial\Phi(x,t)}{\partial x}\right)_{x=0} = 0 \quad (10)$$

(3) Electric-field continuity at the boundary between the compact double layer and the rest of the film (inside the compact double layer the electric field is assumed to be constant):

$$\left(\frac{\partial\Phi}{\partial x}\right)_{x=0} = \frac{\Phi_c^0 - \Phi_c}{d} \quad (11)$$

The potential values at the two contacts are taken to be one-half of the applied voltage:

$$-\Phi_c = \Phi_a = \frac{V_{app}}{2} \quad (12)$$

As previously discussed, the individual charge injection potential barriers are described in terms of the band gap (eq 4).

Several parameters used for simulation need to be estimated first. The band-gap value is taken to be 2.3 V. The total concentration of Ru^{II} sites, c^*, is taken to be $\sim 1.5 \times 10^{-3}$ mol/cm^3.[23] We could not separately measure the diffusion coefficient of the anions, D_a, and the concentration of mobile anions, c_a^0, but a good estimate of their product can be obtained from the zero-bias impedance measurements. If one takes the resistance of the $Ru(bpy)_3(ClO_4)_2$ film at zero-bias to be ∼2 MΩ (Figure 3), and takes into account that if no voltage is applied, the only mobile species are the anions, then the film resistance is

$$R_{film} = \frac{RTL}{F^2 D_a c_a^0 A} \quad (13)$$

where L is the film thickness, c_a^0 is the concentration (uniform throughout the cell) of the mobile ions under no bias, and A is the contact area. In all the simulations the product $D_a c_a^0$ was a constant given by

$$D_a c_a^0 = \frac{RTL}{F^2 A R_{film}} \quad (14)$$

The diffusion coefficients of holes and electrons were assumed to be equal, and their values were taken so that the calculated current would be the same order of magnitude as the experimental current (i.e., ∼100 mA/cm^2). Typically, for ClO_4^- anions, taking the zero-bias resistance to be ∼2 MΩ and

(21) Saveant, J. M. *J. Electroanal. Chem.* **1986**, *201*, 211.
(22) Maness, K. M.; Terrill, R. H.; Meyer, T. J.; Murray, R. W.; Wightman, R. M. *J. Am. Chem. Soc.* **1996**, *118*, 10609.
(23) Ikeda, N.; Yoshimura, A.; Tsushima, M.; Ohno, T. *J. Phys. Chem. A* **2000**, *104*, 6158.

assuming a concentration of mobile ions of ~0.04 mol/L, the diffusion coefficient of the anions would be about 3×10^{-12} cm^2/s. A value of (see Appendix) $\delta_p = \delta_n = D_p/D_a = D_n/D_a =$ 50.000 would give for holes and electrons D_p and D_n values of about 10^{-7} cm^2/s, which are reasonable.[22,24] The thickness of the compact layer near each electrode was estimated to be 0.85 nm. The dimensionless recombination rate constant, R, was taken to be 10^{10} in all simulations, while κ was assumed to be ~57 000 (corresponding, for a 100 nm film, to ~0.04 mol/L mobile ion concentration); all simulation results are presented in dimensionless form only (see Appendix).

Numerical Method. To describe efficiently the large electric-field domains near each electrode, a nonuniform grid was chosen. The film was divided into three regions: two regions near each electrode and one bulk region. In each region near the electrodes an exponential grid was chosen, while in the bulk region the grid was taken as uniform.

The dimensionless flux eqs 5 were made spatially discrete using the Scharfetter−Gummel method,[25] so that on a nonuniform grid, the flux of holes in each box, j, is given by

$$\tilde{f}_{p,j} = -z_p \delta_p \frac{\varphi_{j+1} - \varphi_j}{\xi_{j+1} - \xi_j} \times \left(\frac{p_{j+1}}{1 - e^{-z_p(\varphi_{j+1} - \varphi_j)}} + \frac{p_j}{1 - e^{z_p(\varphi_{j+1} - \varphi_j)}} \right) \quad (15)$$

(Similar expressions can be written for electrons and mobile anions.) This discretization allows for better numerical stability when the fields are large and provided much more accurate profiles as compared to the classical discretization scheme.[25,26] The discretized fluxes were then replaced in the continuity equations and discretized in the time coordinate using a classical Euler scheme.

The resulting algebraic equations were solved using a fully implicit scheme. For each time step the solution at the previous time node was used as the initial guess, and the solution was refined using the Newton method. By taking advantage of the block-tridiagonal structure of the Jacobian matrix, reasonable computing times could be obtained even when the number of grid points was large.[27] A typical run, using 440 grid points for high accuracy, takes less than 200 s on a Pentium III 650 MHz computer. However, 200 grid points may provide enough accuracy for most cases.

Simulation Results. When the voltage is first applied, there is a uniform field across the film given by the applied potential divided by the film thickness. This field is not sufficient to cause charge injection at either electrode. During the first moments following the application of a voltage step, a capacitive (or displacement) current flows through the film due to the movement of the ions very close to the electrode. This leads to a rapid change in the electric-field distribution with an increase in the fields near the electrodes. The current follows an (almost) exponential decay, as expected, reaching very low values quite rapidly. If we assume that the injection barriers favor electron injection, at some point the electric field near the cathode can be large enough for charge to be injected. At this time, the current starts to rise and becomes dominated by the injected carrier current (while the counterions still move and the electric field still continues to change, but the current due to these processes is small). Immediately after the charge has been injected, the electric field in the bulk film is still large enough to contribute significantly to the carrier current. As the counterions and the injected charge move, the electric field in the bulk film decreases, and the current passes through a maximum. After the maximum, the current begins to decrease as the electric field in the bulk film approaches zero, and the migration term becomes negligible. If the electric field at the anode does not reach the value necessary for charge injection, the current decreases steadily toward a steady-state value of the unipolar current (electron injection out of the cathode and into the anode). If, on the other hand, the applied voltage is large enough so that the holes can also be injected, the current will start to rise again as the contribution of the second carrier becomes important, and reaches the steady-state value corresponding to a bipolar current (electron injection at cathode and hole injection at anode with electron−hole recombination occurring in some zone in the film).

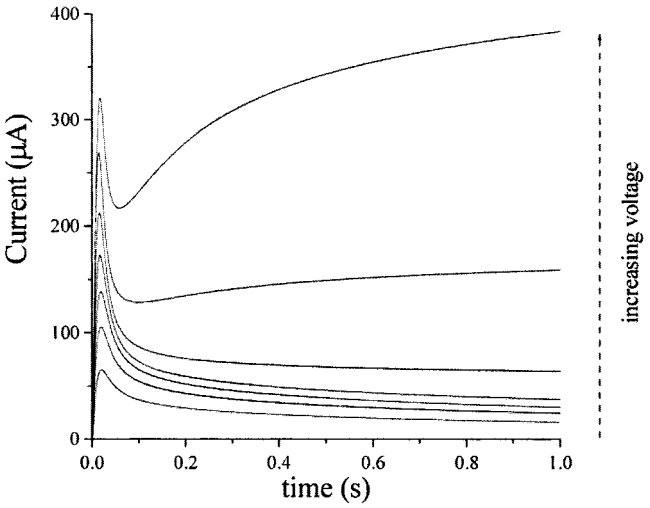

Figure 4. Current transients for a ITO/$Ru(bpy)_3(ClO_4)_2$(100 nm)/GaIn device (contact area ≈ 0.008 cm^2); 2.0, 2.1, 2.2, 2.3, 2.4, 2.5, and 2.6 V.

As discussed above, one can notice several important features in the current transients and current−voltage curves that can be understood from the proposed model. The maximum in the current transient (Figure 4), followed by a gradual rise at higher voltages, is related to nonsymmetrical charge injection at the two electrodes. Although we compare the simulation results only with experimental data for devices made in air, the transients for the drybox devices show similar features. Figure 5 shows the simulated current transients which resemble the experimental transients quite well. The maximum in current during unipolar injection (at low voltages) is specific to space-charge transient currents. It can be explained by the migrational term contribution to the total current, which decreases as the field builds up at the electrode surfaces and decreases to almost zero in the bulk film, so that the current becomes almost entirely diffusional at that time. Similar current transients have been observed for poly(*p*-phenylene-vinylene) in poly(ethylene-oxide)/lithium triflate polymer LECs.[12]

Simulations carried out with equal potential barriers (ν = 0.5 in eq 13) usually do not show such maxima. In this case, holes are injected more efficiently (the mobile anions can

(24) Terrill, R. H.; Murray, R. W. *Mol. Electron.* **1997**, 215.
(25) Scharfetter, D. L.; Gummel, H. K. *IEEE Trans. Electron Devices* **1969**, *ED-16*, 64.
(26) Brumleve, T. R.; Buck, R. P. *J. Electroanal. Chem.* **1978**, *90*, 1.
(27) Rudolph, M. *J. Electroanal. Chem.* **1991**, *314*, 13.

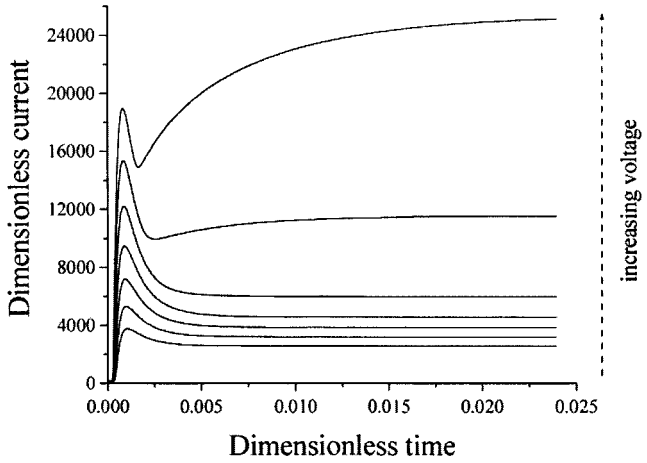

Figure 5. Simulated current transients for a 100 nm device; 2.0, 2.1, 2.2, 2.3, 2.4, 2.5, and 2.6 V. $\delta_p = \delta_n = 50\,000$; $V_b = 2.3$ V; $\nu = 0.375$.

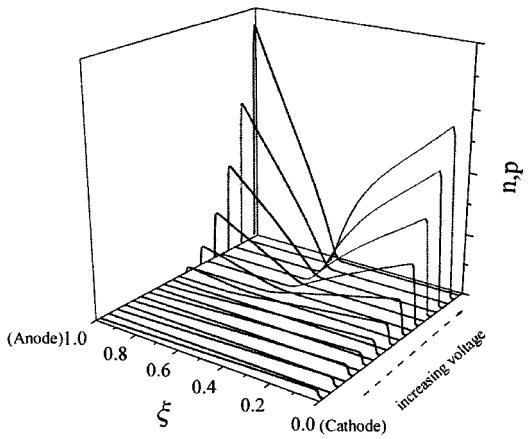

Figure 6. Simulated steady-state electron and hole profiles at different voltages. All other simulation parameters are as in Figure 5.

continue to accumulate near the anode, while the cathodic region becomes depleted of mobile charge). Because the electric field near the anode is not limited by the local ionic concentration, the electric field in the bulk film is always very low. This would imply that the hole current is almost always, mainly, a diffusional one. However, the Poisson equation assumes that all charged species are point charges, and, hence, the concentration of ions can reach very large, physically unrealistic values. At very large applied voltages, saturation effects are expected due to the finite ion size (see, e.g., ref 28).

The simulated current transients resemble the experimental curves only for $\nu < 0.5$, that is, when electrons are injected more efficiently than holes, an assumption supported by the estimated potential barriers (see Table 1). Because only anions are considered to be mobile, the asymmetry in the charge injection is voltage dependent. As the voltage increases, the layer near the cathode becomes totally depleted of mobile anions, because the injected electrons, having very large mobilities as compared to the ions, are "expelled" very rapidly from this high electric-field region. In this circumstance, the local concentration hardly affects the electric field, and holes are injected more and more efficiently (Figure 6). At this point, the conduction becomes bipolar.

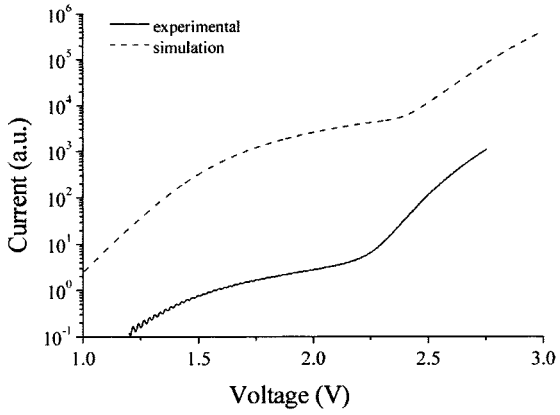

Figure 7. Comparison between the simulated and the experimental current−voltage curves. All other simulation parameters are as in Figure 5.

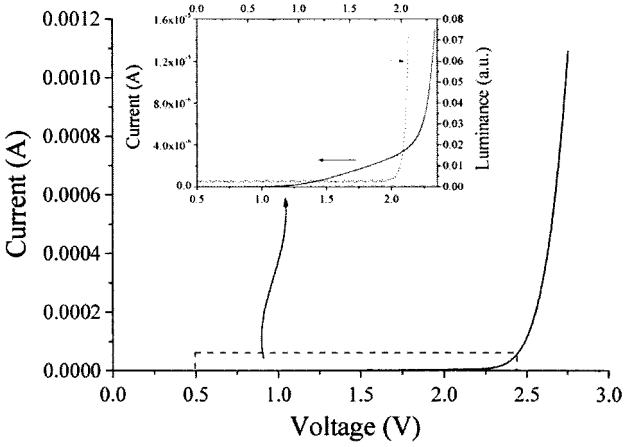

Figure 8. Experimental current−voltage curves (scan rate, 50 mV/s). The inset shows both current and luminance in the low voltage region.

One can see by comparing the experimental and the simulated transients that the experimental current maxima are sharper than the simulated maxima. A possible explanation of this effect may be a field dependence of electron and hole mobilities, as is frequently seen for disordered materials,[29] and which is not accounted for in the simple model here.

Figure 7 shows a comparison between the experimental and the simulated current−voltage curves. While the shape of the simulated curve is essentially the same as that of the experimental curve, the slope of the simulated curve is smaller; that is, the current rises more slowly with the applied voltage, which can also be explained by field-dependent mobilities. However, the presence of a second reduction of the $Ru(bpy)_3^{2+}$ may also lead to a current increase for larger voltages.

The different charge injection can also be observed on the current−voltage curves. Figure 8 shows an experimental current−voltage in which one can notice a change in slope at low voltages. The simulated curve (Figure 9) shows the same appearance. In both cases, light is seen approximately at the point where the slope is changed, indicating that only one electrode reaction takes place significantly at these voltages. Moreover, simulations ran with $\nu \geq 0.5$ did not show such changes in slope. Once again, only by assuming a lower potential barrier for electron injection ($\nu < 0.5$), the simulated curve resembles well the experimental curve.

(28) Borukhov, I.; Andelman, D. *Phys. Rev. Lett.* **1997**, *79*, 435.

(29) Brütting, W.; Berleb, S.; Mückl, A. *Org. Electron.* **2001**, *2*, 1.

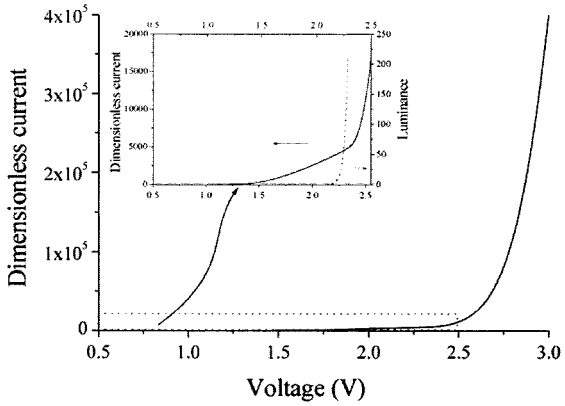

Figure 9. Simulated current−voltage curves (scan rate, 50 mV/s; all other parameters are as in Figure 5). The inset shows both current and luminance in the low voltage region.

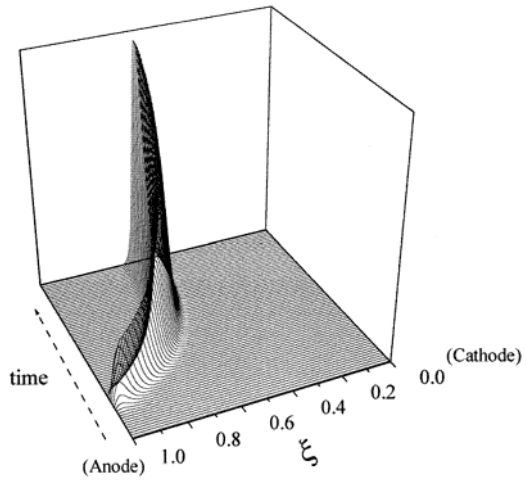

Figure 10. Simulated recombination profiles as a function of time at 2.7 V. All simulation parameters are as in Figure 5.

Figure 10 shows how the recombination profile changes with time at 2.7 V. Note that the recombination maximum is, initially, very close to the anode and moves toward the middle of the film as holes start to inject more efficiently. However, due to the different charge injection at the electrodes, the steady-state recombination profile is still not located exactly in the middle of the film, even though we assumed the mobilities of electrons and holes to be identical.

For applied voltages larger than ca. 2.7 V, the electric field in the bulk film can be large enough to make the migration contribution to the current important at steady state. Simulation results show that the hole profiles are almost perfect straight lines, indicating that the hole current is almost purely diffusional. This is due to the continuous rise of the electric field as a result of anion accumulation near the anode, as previously discussed. In the case of electrons, the profiles are, however, quite different and cannot be considered as straight lines, showing that migration is more important in this case.

It is difficult to obtain more quantitative estimates from this model since little is known about the properties of these films. For example, the model would correctly predict an increase of quantum efficiency as the voltage increases (due to changing from unipolar to bipolar behavior), up to a maximum internal quantum efficiency of 4.6% (based on the fluorescence quantum efficiency of $Ru(bpy)_3^{2+}$ at room temperature), but it does not predict a decrease once the conduction becomes bipolar (as experimentally observed). If one would refine the model and take into account the second and third reduction of $Ru(bpy)_3^{2+}$, as well as side reactions and quenching effects due to the oxidized and reduced species and traces of water present in the film, the decrease in quantum efficiency may be predicted as well, but at the expense of introducing more parameters that are very difficult to estimate or measure. On the other hand, even for the simple model presented here, it is difficult to find good estimates for parameters, and some of the estimates rely on data obtained in solution. For example, the steady-state current depends both on the band gap and on the concentration of mobile ions. A difference of 100 mV in determining the band-gap value, which is within the precision of the estimates, can lead to large changes in the steady-state current. Moreover, the concentration of mobile ions, which is extremely difficult to estimate, determines the magnitude of the electric fields near the electrodes and hence the concentration of injected electrons and holes. This also affects, critically, the steady-state current and luminescence. Nevertheless, we believe that the above simulation results aid in a better understanding of the behavior of these devices.

Conclusions

It is shown that the behavior of tris(2,2′-bipyridine)ruthenium-(II)-based light-emitting devices depends strongly on the nature of mobile ions. Moreover, traces of water in the tris(2,2′-bipyridine)ruthenium(II) film seem to be intimately linked to the existence of mobile ions.

A simple semiquantitative electrochemical model is proposed for describing both the transient and the steady-state behavior of light-emitting devices based on tris(2,2′-bipyridine)ruthenium(II) and light-emitting electrochemical cells in general. The model describes well the transient behavior of these electroluminescent devices, proving that they are, in fact, light-emitting electrochemical cells.

The experimental data correlated with the simulation's results indicate that for low applied voltages, electrons are the main carriers in tris(2,2′-bipyridine)ruthenium(II) light-emitting devices, while for larger voltages, the device becomes bipolar.

Acknowledgment. Support by MURI (DAAD19-01-1-0676), The Center for Nano- and Molecular Science and Technology, and The Robert A. Welch Foundation is acknowledged. The authors wish to thank Stephen Feldberg (Brookhaven National Laboratory) for helpful discussions and David Saunders (NASA Ames Research Center) for providing several Fortran routines.

Appendix

All equations were rewritten in dimensionless form. The dimensionless parameters and variables are film thickness, L; diffusion coefficient of the anions, D_a; time, t; initial concentration of mobile anions, c_a^0; hole and electron concentrations, respectively, c_p, c_n; electric potential, Φ; dielectric permittivity of vacuum and the relative dielectric constant of the film, respectively, ϵ_0, ϵ; second-order recombination rate constant, k; dimensionless space coordinate, $\xi = x/L$; dimensionless time coordinate, $\tau = D_a t/L^2$; dimensionless concentrations for coun-

terions, holes, and electrons, respectively, $a = c_a/c_a^0$, $p = c_p/c_a^0$, $n = c_n/c_a^0$; dimensionless electric potential, $\varphi = F/RT \times F$; the ratio between the diffusion coefficients of holes and anions and electrons and anions, respectively, $\delta_p = D_p/D_a$, $\delta_n = D_n/D_a$; dimensionless recombination rate constant, $R = kc_a^0L^2/D_a$; dimensionless parameter related to the Debye length, $\kappa = F^2L^2c_a^0/RT\epsilon\epsilon_0$; dimensionless current, $\tilde{I} = \sum_{i=p,n,a} \tilde{f}_i - (1/\kappa)(\partial/\partial\tau)(\partial\varphi/\partial\xi)$, where $\tilde{I} = IL/(FD_ac_a^0A)$, A is the contact area, and $\tilde{f}_i$ are the dimensionless fluxes (eq 5).

Supporting Information Available: Discretization and numerical model (PDF). This material is available free of charge via the Internet at http://pubs.acs.org.

JA017834H

Supporting Information:

Potential drops within the film:

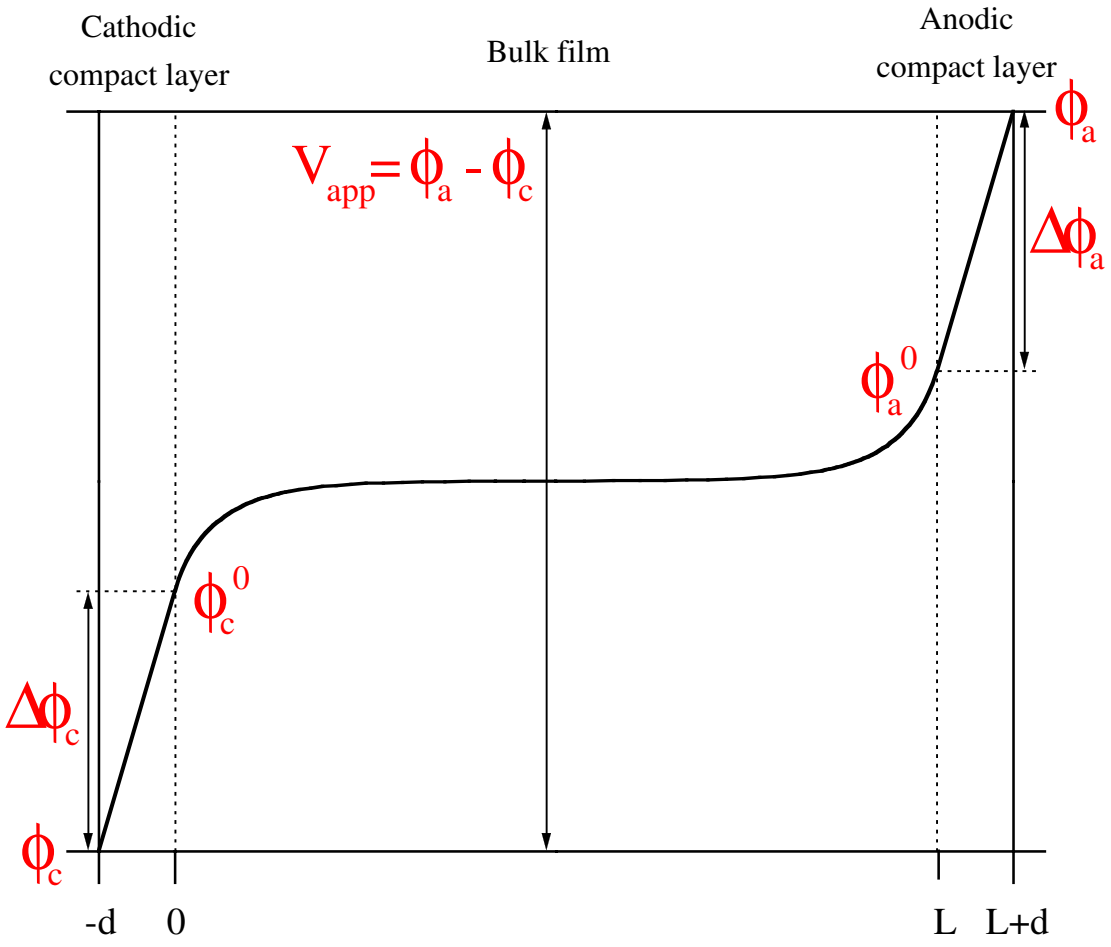

Figure SI-1. Potential distribution in the Gouy-Chapman-Stern model of the Ru(II)$(bpy)_3$ film.

The film extends from 0 to L; the compact double-layers near the electrodes are taken from 0 to –d (cathode) and from L to L+d (anode). Inside the compact layer (its thickness would correspond to a monolayer of $Ru(bipy)_3^{2+}$) the potential drop is considered to be linear.

Discretization and numerical model

We chose a non-uniform grid, as in Figure 2. The regions near each electrode, where an exponential grid was used, are about 5 Debye lengths thick, where the Debye length, l_D is:

$$l_D = \frac{1}{F}\sqrt{\frac{2RT\varepsilon\varepsilon_0}{c}}$$

where *c* is the concentration of mobile ions; all other parameters have the usual significance.

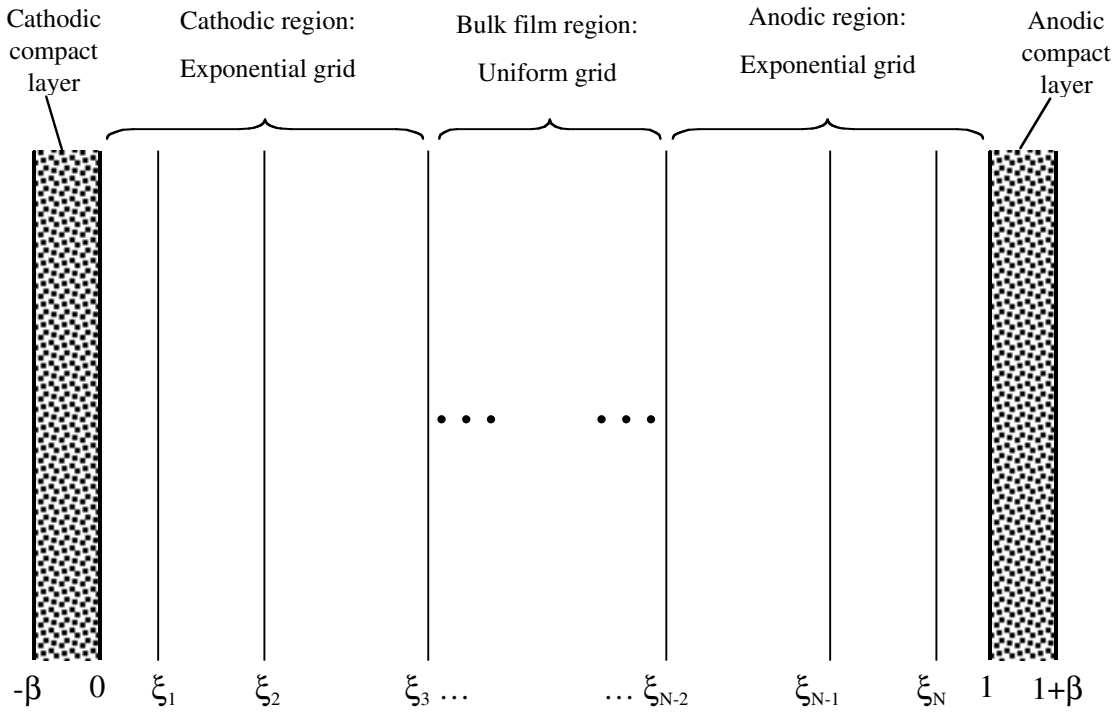

Figure SI-2. Spatial discretization scheme of the Ru(II)$(bpy)_3$ film.

We also chose a non-uniform, exponentially expanding, time grid, so that for small times when the changes in electric field are fast, small time increments are used. An example of a time expanding grid can be found in ref. 1. Since this is a stiff set of equations, we used an Euler, fully implicit scheme for time discretization:

$$\frac{c_{ij}^{\tau+\Delta\tau} - c_{ij}^{\Delta\tau}}{\Delta t} = -\frac{f_{ij+1}^{\tau+\Delta\tau} - f_{ij}^{\tau+\Delta\tau}}{\Delta x_j} \qquad \text{(SI-1)}$$

After choosing the grid, one can write eqs.(5) – (7) and the boundary conditions (9) – (11) in dimensionless form:

$$\tilde{f}_p(\xi,\tau) = -\delta_p\left(\frac{\partial p(\xi,\tau)}{\partial\xi} + z_p p(\xi,\tau)\frac{\partial\varphi(\xi,\tau)}{\partial\xi}\right);\ \frac{fp(\xi,\tau)}{f\tau} = -\frac{f\tilde{f}_p(\xi,\tau)}{f\xi} - R \leftrightarrow pn \qquad \text{(SI-2)}$$

$$\tilde{f}_n(\xi,\tau) = -\delta_n\left(\frac{\partial n(\xi,\tau)}{\partial\xi} + z_n n(\xi,\tau)\frac{\partial\varphi(\xi,\tau)}{\partial\xi}\right);\ \frac{fn(\xi,\tau)}{f\tau} = -\frac{f\tilde{f}_n(\xi,\tau)}{f\xi} - R \leftrightarrow pn \qquad \text{(SI-3)}$$

$$\tilde{f}_a(\xi,\tau) = -\left(\frac{\partial a(\xi,\tau)}{\partial\xi} + z_a a(\xi,\tau)\frac{\partial\varphi(\xi,\tau)}{\partial\xi}\right);\ \frac{fa(\xi,\tau)}{f\tau} = -\frac{f\tilde{f}_a(\xi,\tau)}{f\xi} \qquad \text{(SI-4)}$$

$$\frac{f^2\varphi(\xi,\tau)}{f\xi^2} = \kappa(n - p + a - 2) \tag{SI-5}$$

where $\xi = x/L$; $\tau = D_a t/L^2$; $a = c_a/c_a^0$; $p = c_p/c_a^0$; $n = c_n/c_a^0$; $\varphi = F/RT\times\Phi$; $\delta_p = D_p/D_a$; $\delta_n = D_n/D_a$; $R = kc_a^0L^2/D_a$; $\kappa = F^2L^2c_a^0/RT\varepsilon\varepsilon_0$ (c_a^0 represents the concentration of mobile anions).

The dimensionless current is given by:

$$\tilde{I} = \sum_{i=p,n,a}\tilde{f}_i - \frac{1}{\kappa}\frac{\partial}{\partial\tau}\left(\frac{\partial\varphi}{\partial\xi}\right) \tag{SI-6}$$

where $\tilde{I} = IL/(FD_ac_a^0A)$ and A is the contact area. Note that the total current is negative, but its sign is just a matter of convention.

The dimensionless form of the boundary conditions are given by:

$$\Delta\varphi_c = \varphi_c - \varphi_0 = e_c^0 + \ln\left(\frac{\delta_c - n(0,t) - p(0,t)}{n(0,t)}\right) = e_a^0 + \ln\left(\frac{p(0,t)}{\delta_c - n(0,t) - p(0,t)}\right) \tag{SI-7}$$

$$\left(\frac{\partial a(\xi,\tau)}{\partial\xi}\right)_{\xi=0} - a(0,\tau)\times\left(\frac{\partial\varphi(\xi,\tau)}{\partial\xi}\right)_{\xi=0} = 0 \tag{SI-8}$$

$$\left(\frac{\partial\varphi}{\partial\xi}\right)_{\xi=0} = \frac{\varphi_0 - \varphi_c}{\beta} \tag{SI-9}$$

$$\Delta\varphi_a = \varphi_a - \varphi_{N+1} = e_c^0 + \ln\left(\frac{\delta_c - n(1,t) - p(1,t)}{n(1,t)}\right) = e_a^0 + \ln\left(\frac{p(1,t)}{\delta_c - n(1,t) - p(1,t)}\right) \tag{SI-10}$$

$$\left(\frac{\partial a(\xi,\tau)}{\partial\xi}\right)_{\xi=1} - a(1,\tau)\times\left(\frac{\partial\varphi(\xi,\tau)}{\partial\xi}\right)_{\xi=1} = 0 \tag{SI-11}$$

$$\left(\frac{\partial\varphi}{\partial\xi}\right)_{\xi=1} = \frac{\varphi_a - \varphi_{N+1}}{\beta} \tag{SI-12}$$

where $\delta_c = c^*/c_a^0$ and $\beta = d/L$ (c^* is the total concentration of the Ru(bipy)$^{2+}$ sites).

For calculating the excited-state concentration profiles with time, one more equation is needed (written in dimensionless form):

$$\frac{f\gamma}{f\tau} = \delta_\gamma\frac{f^2\gamma}{f\xi^2} + R\leftrightarrow pn - k\leftrightarrow\gamma \tag{SI-13}$$

where γ is the dimensionless excited state concentration (c^*/c_a^0), δ_γ is the dimensionless diffusion coefficient of the excite state (D_*/D_a) and k is the dimensionless decay constant of the excited state ($k_d\times L^2/D_a$).

However, this equation can be solved independently once the electron and hole profiles are known and does not require special treatment. The total electroluminescent light (expressed

as number of photons per second) coming out from the film will be:

$$P = N_A \frac{AD_a c_a^0}{L} \times k \int_0^1 y d\xi \qquad \text{(SI-14)}$$

where N_A is Avogadro's number.

A classical discretization scheme does not work for this problem: the electric fields near the electrodes (mostly near the anode, where mobile anions can accumulate; near the cathode, a classical scheme might be used, although a large number of points are still needed) change very rapidly with distance, and the classical discretization scheme fails (even 2000 points in the anodic region are not enough to achieve convergence). Therefore, one needs to carefully choose the numerical procedure. One of the most successful and widely used for semiconductor simulations is the Scharfetter-Gummel discretization procedure, which works very well for very large electric fields (although it fails when the electric field is very low). The Scharfetter-Gummel method does not evaluate the partial derivatives of concentrations and potential as first order approximations in one box, but instead assumes that within one box all the fluxes and the electric field are constant. For example, in the flux equation for holes:

$$\tilde{f}_p(\xi,\tau) = -\delta_p \left(\frac{\partial p(\xi,\tau)}{\partial \xi} + z_p p(\xi,\tau) \frac{\partial \varphi(\xi,\tau)}{\partial \xi} \right)$$

if the flux $\tilde{f}_p(\xi,\tau)$ and $\tilde{e} = \frac{f\varphi(\xi,\tau)}{f\xi}$ are constant, then one can integrate the flux equation in one box:

$$\tilde{f}_p = -\delta_p \left(\frac{dp}{d\xi} + z_p p \tilde{e} \right); \; -\int_j^{j+1} \frac{dp}{z_p p \tilde{e} + \tilde{f}_p / \delta_p} = \int_j^{j+1} d\xi = \xi_{j+1} - \xi_j$$

and obtains:

$$\frac{\tilde{f}_p}{\delta_p} = z_p \tilde{e} \left[\frac{p_j \times \exp(-z_p \tilde{e}(\xi_{j+1} - \xi_j))}{1 - \exp(-z_p \tilde{e}(\xi_{j+1} - \xi_j))} - \frac{p_{j+1}}{1 - \exp(-z_p \tilde{e}(\xi_{j+1} - \xi_j))} \right] =$$

$$= -z_p \tilde{e} \left[\frac{p_j}{1 - \exp(z_p \tilde{e}(\xi_{j+1} - \xi_j))} + \frac{p_{j+1}}{1 - \exp(-z_p \tilde{e}(\xi_{j+1} - \xi_j))} \right]$$

By replacing $\tilde{e} = \frac{f\varphi}{f\xi} = \frac{\varphi_{j+1} - \varphi_j}{\xi_{j+1} - \xi_j}$, eq. (15) is obtained:

$$\tilde{f}_{p,j} = -z_p \delta_p \frac{\varphi_{j+1} - \varphi_j}{\xi_{j+1} - \xi_j} \times \left(\frac{p_{j+1}}{1 - e^{-z_p(\varphi_{j+1} - \varphi_j)}} + \frac{p_j}{1 - e^{z_p(\varphi_{j+1} - \varphi_j)}} \right) \qquad \text{(SI-15)}$$

Similar expressions can be written for electrons and mobile anions just by changing the letter *p* with *n* and *a* respectively. Note that this procedure does not work if one uses the (more general) Savéant equations for the fluxes: by integrating the flux equation a transcedental

equation is obtained, from which an analytical expression for the flux cannot be obtained. If, however, the carrier concentrations are small compared to the total concentration of redox sites, using the Nernst-Planck equations is a good approximation.

By using this scheme, one achieves very good convergence and accuracy for large fields; in fact 200 grid points (50 near each electrode and 100 for the bulk) may be enough for most situations (depending on the concentration of mobile ions: for large concentrations, a larger number of grid points might be needed). One can easily notice that this procedure fails if the electric field is very low: the exponentials in the flux expression tend to 1 when the electric field is small, and a division by zero occurs. Depending on the precision with which the exponential is evaluated, the lowest voltage value at which the algorithm is still usable may vary. In our case, the algorithm ceases to work for applied voltages lower than ~0.6 V. A series expansion of the exponentials in eq. SI-15 may extend the validity region for small voltages too.

The flux equations are then replaced in eq. (SI-1) written in dimensionless form. One obtains a set of equations that can be written as:

$$F_{j\varphi}(\varphi, n, p, a) = 0 \quad \text{(SI-16)}$$

$$F_{jn}(\varphi, n, p, a) = 0 \quad \text{(SI-17)}$$

$$F_{jp}(\varphi, n, p, a) = 0 \quad \text{(SI-18)}$$

$$F_{ja}(\varphi, n, p, a) = 0 \quad \text{(SI-19)}$$

where the j index represents the j-th grid point, while index $i = \varphi, n, p, a$ indicate the variable (potential, and chemical species). For the first and the last grid points, the boundary conditions (SI-7) to (SI-12) are replaced in the expressions of each F_{1i} and F_{Ni}, so one obtains a system of non-linear equations of order 4N (N is the number of the grid-points; the cathode is chosen at grid point 0 and the anode at N+1). Now one can choose a method for solving this system: the most widely used is the Newton-Raphson method, which ensures fast convergence. If one has a system of equations written as:

$$\mathbf{F}(\mathbf{X}) = 0 \quad \text{(SI-20)}$$

where $\mathbf{F}$ is the functions vector and $\mathbf{X}$ is the variables vector, then at each iteration, k, the solution is improved by using the following procedure:

$$\mathbf{X}^{k+1} = \mathbf{X}^k + \Delta\mathbf{X}^k;\ \Delta\mathbf{X}^k = -(\mathbf{J}^k)^{-1}\times\mathbf{F}^k \quad \text{(SI-21)}$$

where $\mathbf{J}$ is the Jacobian matrix:

$$\mathbf{J} = \begin{bmatrix} \frac{\partial F_1}{\partial X_1} & \frac{\partial F_1}{\partial X_2} & \cdots & \frac{\partial F_1}{\partial X_N} \\ \frac{\partial F_2}{\partial X_1} & \frac{\partial F_2}{\partial X_2} & \cdots & \frac{\partial F_2}{\partial X_N} \\ \cdots & \cdots & \cdots & \cdots \\ \frac{\partial F_N}{\partial X_1} & \frac{\partial F_N}{\partial X_2} & \cdots & \frac{\partial F_N}{\partial X_N} \end{bmatrix} \tag{SI-22}$$

The easiest way to use the Newton-Raphson for this kind of problem is to use the solution from the previous time moment as an initial guess (for the first time step, the initial condition is used as a guess) and improve the solution until $\sum \Delta X_{ji}$ is less than some expected tolerance value. For our specific problem, the **F** vector represents the set of equations (SI-16) through (SI-19), and the variables vector **X** represents the potential, electron hole and anion concentrations at each grid-point (φ_j, n_j, p_j, a_j).

Each Newton-Raphson iteration requires the inverse of the 4N×4N Jacobian matrix. If the number of grid points is large, the inversion is a very expensive process and the whole algorithm becomes very slow. However, it is easy to see that by grouping all functions $F_{j\varphi}$, F_{jn}, F_{jp} and F_{ja} at the same grid point, the resulting Jacobian matrix is a block-tridiagonal matrix in which each block has a 4×4 size:

$$\mathbf{J} = \begin{bmatrix} [B_{11}] & [B_{12}] & 0 & 0 & 0 & \cdots & 0 \\ [B_{21}] & [B_{22}] & [B_{23}] & 0 & 0 & \cdots & 0 \\ 0 & [B_{31}] & [B_{32}] & [B_{33}] & 0 & \cdots & 0 \\ \cdots & \cdots & \cdots & \cdots & \cdots & \cdots & \cdots \\ 0 & \cdots & 0 & [B_{N-2N-3}] & [B_{N-2N-2}] & [B_{N-2N-1}] & 0 \\ 0 & \cdots & 0 & 0 & [B_{N-1N-2}] & [B_{N-1N-1}] & [B_{N-1N}] \\ 0 & \cdots & 0 & 0 & 0 & [B_{NN-1}] & [B_{NN}] \end{bmatrix} \tag{SI-21}$$

This feature is an immediate consequence of the linear approximation of the derivatives: for a second order derivative, the functions F_{ji} depend only on the variables evaluated at the j-1, j and j+1 grid points, so the derivatives, with respect to the rest of variables, are zero. The first and last line of the Jacobian contain only two terms because the variables at 0 (cathode) and N+1 (anode) are not independent, but can be written as functions of the variables at points 1 and N respectively, from the boundary conditions.

Inverting a block-tridiagonal matrix requires less CPU time; special algorithms for inverting block-tridiagonal matrices can be found in many free linear-algebra software packages. It is always better to provide an analytical Jacobian, but if one considers that the analytical derivation is too cumbersome, a numerical Jacobian may be used as well. If, however, one is interested in fast computation, the analytical Jacobian may sometimes save 10-20% CPU time.

A complete algorithm for solving the above presented problem may look as follows:

[1]. Choose a spatial grid and calculate the grid points;

[2]. Choose a time grid;

[3]. For each increment $\Delta\tau$, take the solution at time step τ and perform one Newton-Raphson iteration;

[4]. Calculate the $\Delta\mathbf{X}$ vector and compare $\sum \Delta X_{ji}$ with the tolerance;

[5]. If $\sum \Delta X_{ji}$ is larger than the desired tolerance, calculate the new solution vector, **X**, from eq. (SI-21) and go back to [3]. If $\sum \Delta X_{ji}$ is less than the desired tolerance, keep the solution vector **X** as the final solution for time $\tau + \Delta\tau$;

[6] Calculate currents, electric fields and other needed quantities for time τ

[7] Go back to [3] to further increment the time, and use the values for time τ as initial guess until the final desired time value is reached.

The best and easiest way to check the results is to calculate the total current (eq. SI-6): it can be shown that the *total* current *must* be position independent, *i.e.* the total current is a function of time only. If the results do not show a constant total current throughout the film, the program needs to be checked.

Some other results obtained from the simulation are also shown below:

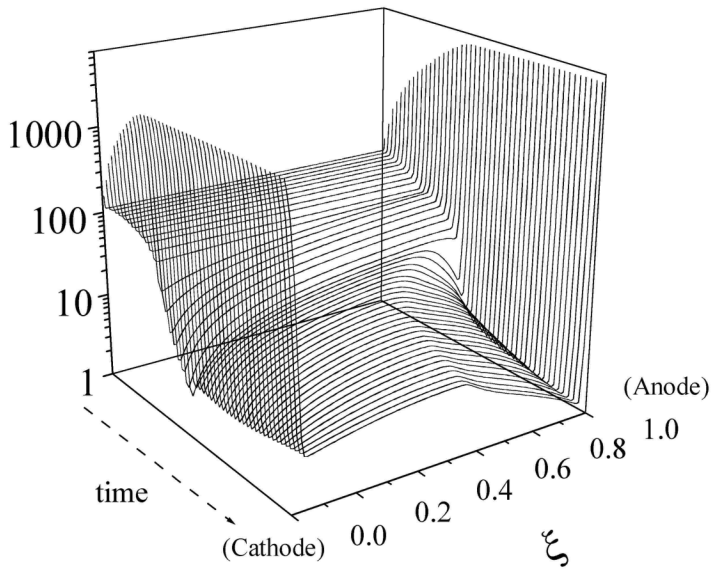

Figure SI-3. Simulated electric field profile within the film at 3.0 V. All other simulation parameters as in Figure 5 from manuscript.

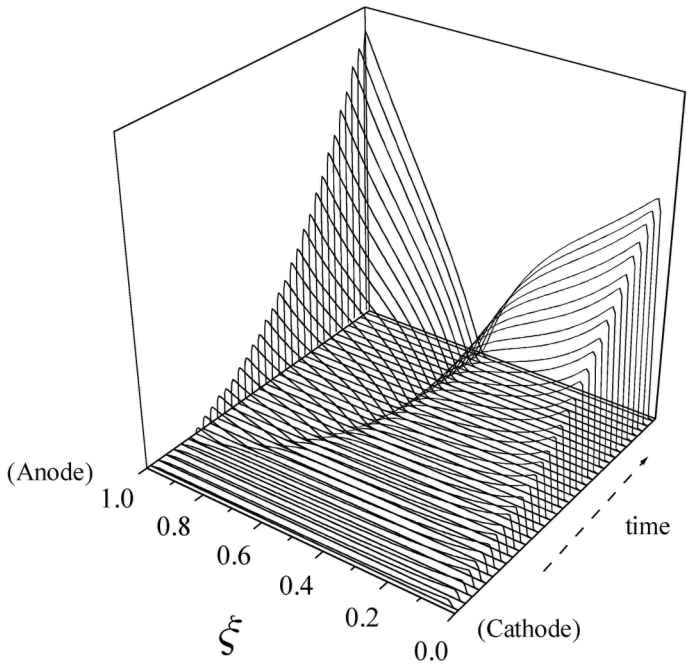

Figure SI-4. Simulated electron and hole profiles as function of time at 3.0 V. All other simulation parameters as in Figure 5 from manuscript.

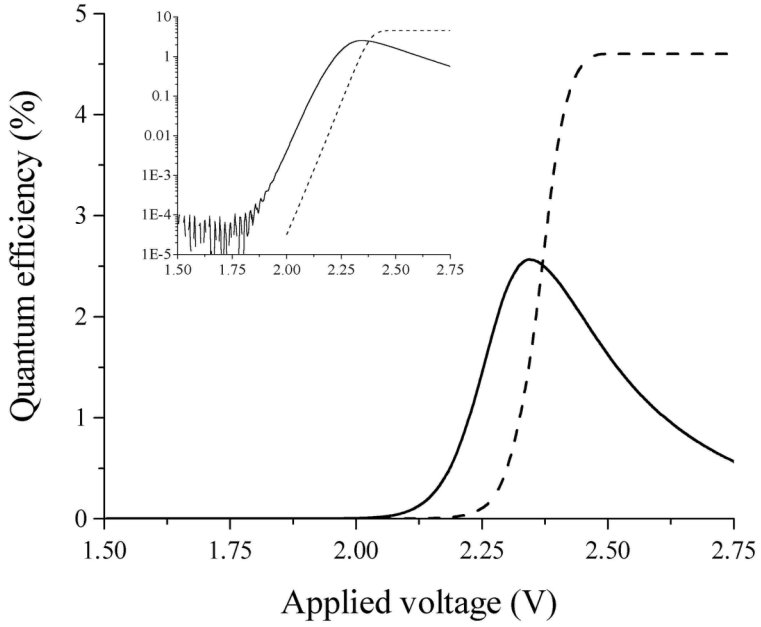

Figure SI-5. Experimental and simulated quantum efficiencies as a function of voltage. All simulation parameters as in Figure 5 from manuscript. Inset shows the same plot, but on a logarithmic scale.

Reference

1 T. R. Brumleve and R. P. Buck, *J. Electroanal. Chem.*, **1978**, *90*, 1.